Case History

3D inversion of a scalar radio magnetotelluric field data set

Gregory A. Newman*, Stephan Recher‡, Bülent Tezkan‡, and Fritz M. Neubauer‡

ABSTRACT

A radio magnetotelluric (MT) field data set, acquired in scalar mode, over a buried waste site has been successfully analyzed using a 3D MT inversion scheme using nonlinear conjugate gradients. The results of this analysis demonstrate the utility of the scheme where more than 4800 data points collected on multiple measurement profiles have been inverted simultaneously. The resulting image clearly detects the buried waste; when receiver profiles cross pit boundaries, the image maps the lateral extent of the pit. However, the base of the pit is poorly resolved, and depends upon the starting model used to launch the inversion. Hence, critical information on whether contamination is leaching into a resistive gravel bed lining the base of the pit, as well as the deeper geological horizons consisting of brown coal, clay, and tertiary sands, is inconclusive. Nevertheless, by incorporating within the inversion process a priori information of the background media that is host to the waste, sharper images of the base of the pit are obtained, which are in good agreement with borehole data. The 3D analysis applied in this paper overcomes previous limitations in the radio magnetotelluric (RMT) method using 2D data analysis and inversion. With 3D analysis, it is unnecessary to make assumptions regarding geological strike, and near-surface statics can be accommodated in both source polarizations. Our findings also indicate that 2D MT interpretation can overestimate the pit's depth extent. This may lead to the erroneous conclusion that the geological horizons beneath the pit have been contaminated.

INTRODUCTION

Increasing speed and memory capability of computers has allowed for the development of magnetotelluric (MT) inversion algorithms that more accurately take into account the three dimensionality of the MT interpretation problem. One example of such a scheme is reported by Newman and Alumbaugh (2000). To image large-scale data sets needed for 3D subsurface imaging, this scheme uses an efficient nonlinear conjugate gradient search to determine the optimal solution. It also uses massively parallel computing architectures to allow for large model parameterizations required for realistic 3D MT modeling and inversion. While this scheme has been developed using synthetic data-set examples and has proved useful in experiment design (Newman et al., 2002), it has not yet been applied successfully to a field data set.

In this paper we apply the 3D MT inversion algorithm discussed above to a radio magnetotelluric (RMT) data set acquired over a buried waste site in Germany. Because measurements were acquired along multiple profiles and are of sufficient quality and density, this data set offers an excellent opportunity to apply the 3D MT inversion algorithm on an actual field example.

Before presenting these results, however, the motivation for waste-site characterization is discussed. Two brief sections describing details of the RMT method and the 3D MT inversion scheme are then covered. Next, a simple model of the waste site is proposed to (1) demonstrate the accuracy of the 3D inversion scheme, (2) ascertain critical features of the model we can and cannot expect to recover within the inversion process when the field data are analyzed, and (3) illustrate some errors that can arise with a 2D interpretation of selected data profiles acquired over the 3D waste site. It turns out that these errors are also observed in the 2D interpretation of the field data.

WASTE-SITE CHARACTERIZATION

Buried waste sites represent a critical environmental problem confronting the European community, as well as other countries throughout the world. For example, during the past 50 years in Germany, small gravel pits have been filled with household refuse, building debris, and different kinds of potentially dangerous industrial waste. These waste sites may impose a significant risk to the environment since they can be a source of groundwater contamination. Hence, a comprehensive monitoring program is necessary to limit the impact these sites may have on the environment.

Commonly, shallow boreholes covering a site have been used for monitoring, but such an approach is expensive and provides only a limited view of the state of the subsurface hydrology and the lateral extent of the waste. One way to obtain additional information on such properties away from boreholes, in a fast and effective way, is to use geophysical methods (see Pellerin and Alumbaugh, 1997; Green et. al., 1999; De Iaco et al., 2000). Often, the electrical conductivity of waste sites is much higher than the surrounding host material. Therefore, electromagnetic (EM) methods can be very suitable for delineating the lateral extent of these sites. Moreover, by repeated measurements, EM methods can also provide a means to monitor changes in the conductivity of the host material—changes that may be correlated to groundwater contamination originating from the waste (see Greenhouse and Slaine, 1983).

THE RMT METHOD

The RMT method is an emerging geophysical mapping technique for waste-site characterization and groundwater investigations (see Zacher et al., 1996; Tezkan et al., 2000). It is being applied in Europe but far less so in North America; hence it is not as well known. The method is an extension of the very-low-frequency (VLF) EM induction method (10–30 kHz) (McNeill and Labson, 1991) to frequencies as high as 1 MHz (Tezkan, 1999). The principle of the method is demonstrated in Figure 1. In the far-field of a radio transmitter, the EM field can be viewed as a propagating plane wave where the horizontal electric and magnetic field components are altered by variations in the subsurface electrical conductivity. In the method, the horizontal magnetic field is measured along with an orthogonal component of the horizontal electric field. With this
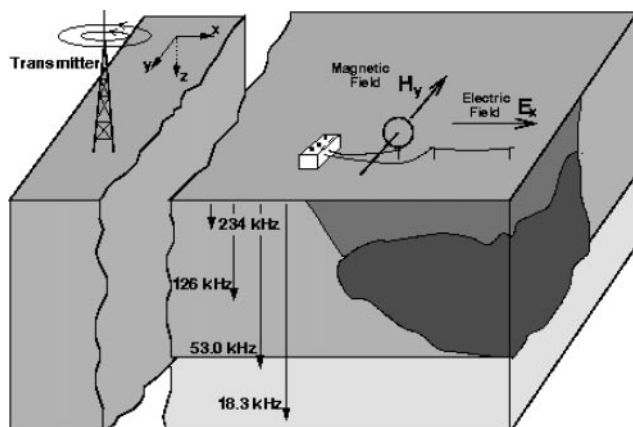

FIG. 1. The RMT survey configuration. Lower frequencies are associated with deeper penetration depths.

measurement the impedance, which is a ratio between particular components of the magnetic and electric field, can be estimated. Because impedance data are ratios of electric to magnetic field, the source location and strength need not be considered further, which greatly simplifies data interpretation. The impedance is usually converted to apparent resistivity and phase at each measurement site using the Cagniard formula in magnetotellurics (Cagniard, 1953; Vozoff 1972, 1991). This transformation allows the measurements to be related more easily to the subsurface geology. Nevertheless, the same information content is present in the impedance data. Because of the use of several frequencies between 10 kHz and 1 MHz, a quick sounding is possible by this method; such soundings using VLF frequencies are impractical because of the method's limited frequency range (10–30 kHz). RMT surveys have been successfully applied in a number of hydrological (Turberg et al., 1994) and environmental investigations (Tezkan et al. 1996; Zacher et al., 1996; Tezkan et al., 2000).

For our field measurements, the RMT instrument was developed from a prototype built at the Hydrogeological Institute of the University of Neuchatel, Switzerland (Mueller, 1983). The horizontal component of the magnetic field is measured with a coil (0.4 m diameter), and the horizontal component of the electric field is measured with two grounded electrodes 5 m apart. The frequency range of this instrument is limited to 10–300 kHz. The instrument is lightweight and easy to use— one important reason for its emerging popularity in environmental applications. Measurements (i.e., apparent resistivity and phase observations from a single radio transmitter) can be carried out in a relatively short time. About two minutes are necessary to measure apparent resistivities and phase values for four frequencies at one fixed location.

Because of the large number of radio transmitters (especially in Europe), it is possible to cover the entire frequency range required for a sounding with selected frequency pairs arising from two orthogonal transmitters. In an ideal case, each pair of transmitters should operate at similar frequencies, where the electric-field polarization of one transmitter is parallel and the other is perpendicular to the general strike direction of the geological or anthropological structure. Assuming a 2D resistivity structure in the survey area, the data can then be associated with the transverse electric and transverse magnetic modes (see Tezkan et al., 1996) and interpreted using standard 2D MT inversion algorithms (see Smith and Booker, 1991; Rodi and Mackie, 2001). Because the instrument treats the data arising from each transmitter, in a given pair, as separate, the Z_{xy} and Z_{yx} impedance measurements are assumed to be independent of each other and the Z_{xx} and Z_{yy} impedances are assumed to be zero and are not measured.

In practice, the strike direction of the target is often unknown. Further complicating matters is the distinct possibility that the target is three dimensional in character. It is then impossible to define geological strike. In these situations, the 2D interpretation procedures outlined above will result in a biased model, providing the motivation for applying 3D MT inversion to such data sets as presented in this paper.

THE FIELD SITE

Our field data come from a waste site near Cologne. This site was a former gravel pit; it is now filled with different kinds

of industrial waste and household refuse. A surface map of the site is illustrated in Figure 2. Here, the solid line indicates the border of the waste site. The waste pit itself is 550 m long with a maximum width of 270 m, and it is covered by a soil
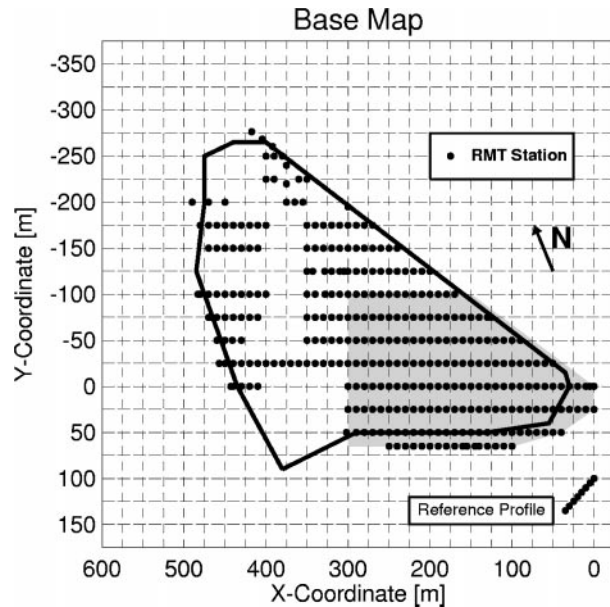

FIG. 2. Base map of the survey area. The black line indicates the lateral boundary of the pit. The gray area shows the region that corresponds to the apparent resistivity and phase maps in Figure 4.

layer that is several meters thick. Borehole data indicate the base of the pit is at approximately 13 m depth. Figure 2 also shows the locations of the RMT measurement stations used in the survey. For logistical reasons (earth walls surrounding the site, vegetation), not all of the measurement profiles cross the boundary of the pit. Regional geological maps of the area (Figure 3) also indicate that the pit rests upon a bed of gravel and coarse sand, below which sits a conductive horizon of clay, brown coal, and tertiary sand beds. These basal units extend well beyond the pit boundaries.

For the field site under investigation, 320 such RMT measurements were taken. At every measurement, eight frequencies were used to cover the range between 234 and 18.3 kHz. Two radio transmitters (transmitter directions, not to be confused with a single transmitter) were used with orthogonal source polarizations, one parallel and the other perpendicular to the assumed strike direction over the measurement site. Only scalar measurements were conducted. Hence, the data were acquired under the assumption that the geology is two dimensional. Given the 3D nature of the field site, this assumption may not be appropriate, as discussed later.

Figure 4 gives an overview of the lateral distribution of the apparent resistivity and phases for a selected frequency of 234 kHz over part of the waste (see the gray area in Figure 2), where the electric field is polarized along the x-direction. Here the waste is indicated when the apparent resistivity ρ_a is less than 40 ohm-m. The lateral border of the waste site with respect to the undisturbed geology, $\rho_a > 100$ ohm-m, can only be seen in the southeastern part of the area; $y \geq 0$ m and $x \leq 100$ m. The phase map shows the crossing of the undisturbed geology
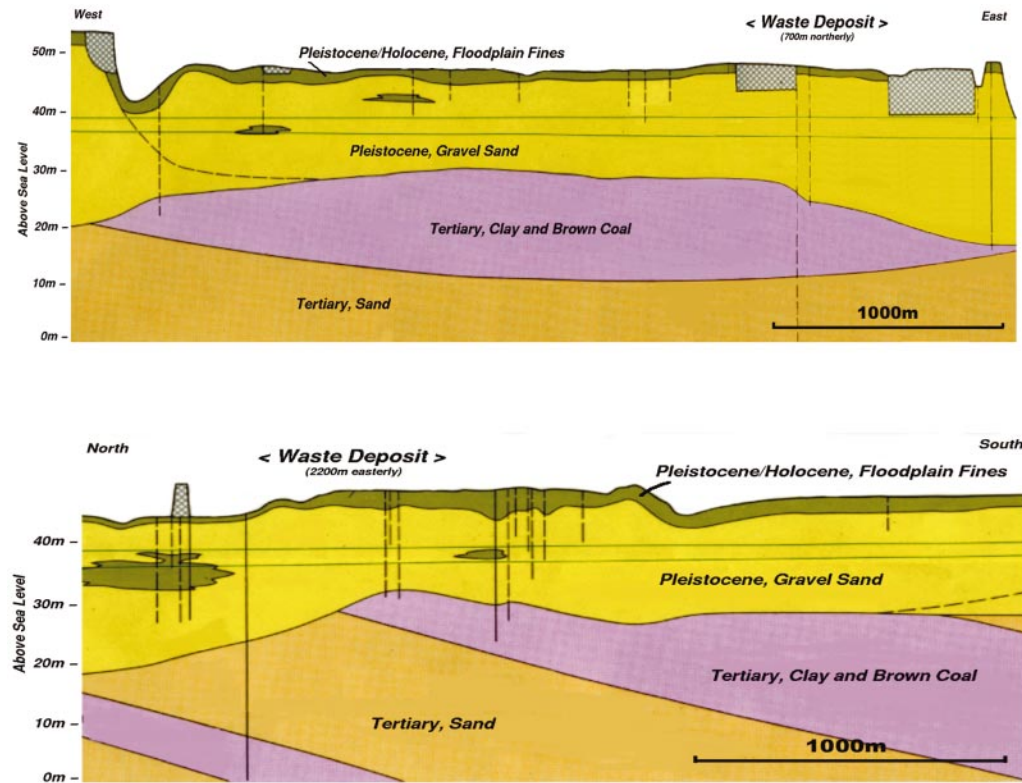

FIG. 3. Geological cross-sections are shown, illustrating the background units housing the waste deposit which is out of plane, 700 m to the north in the top east–west cross-section and 2200 m to the east in the north–south cross-section. Modified from geological maps provided by Geologisches Landesamt NRW (1986).

to the waste pit with an increase in phase from 35° to more than 55°.

THE 3D MT INVERSION ALGORITHM

Following, we give a cursory description of the 3D MT inversion algorithm to be used in the analysis of the waste-site data. Additional details on this algorithm can be found in Newman and Alumbaugh (2000). Following their work, we divide the 3D earth into M prismatic cells and assign to each cell an unknown conductivity value. Let **m** be a vector of length M that describes these values. The regularized least-squares cost functional to be minimized in the inversion process, which combines the data error and model smoothness constraint, is given by

$$\varphi = \{\varepsilon^{-1}(\mathbf{Z^{obs}} - \mathbf{Z^{pre}})\}^{\mathcal{H}}\{\varepsilon^{-1}(\mathbf{Z^{obs}} - \mathbf{Z^{pre}})\} + \lambda\mathbf{m}^T\mathbf{W}^T\mathbf{W}\mathbf{m},$$
(1)

where $\mathcal{H}$ denotes the Hermitian operator. In equation (1), $\mathbf{Z^{obs}}$ and $\mathbf{Z^{pre}}$ are data vectors that represent the predicted and observed MT impedances at different frequencies and locations. These are complex values, and a given entry in the data vector can represent any component of the impedance tensor,

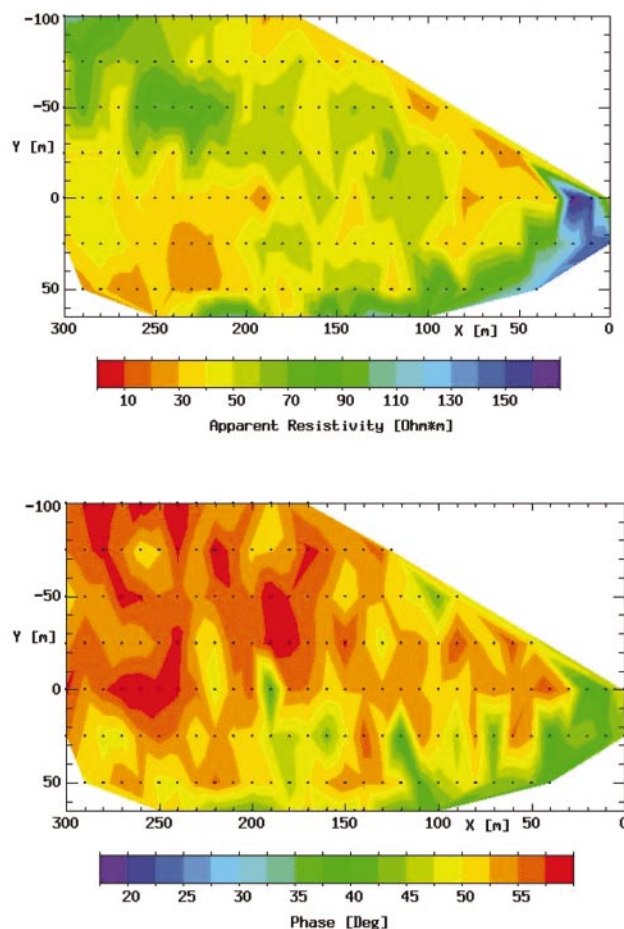$$\mathbf{Z} = \begin{pmatrix} Z_{xx} & Z_{xy} \\ Z_{yx} & Z_{yy} \end{pmatrix},$$
(2)

FIG. 4. Apparent resistivity and phase maps over part of the survey area, corresponding to the gray area in Figure 2.

where ε^{-1} in equation (1) is a diagonal matrix that contains the inverse of the data error estimates. Here, noisier data are given smaller weight, or less importance, when forming φ than good quality data.

The regularization parameters that stabilize the inverse problem (Tikhonov and Arsenin, 1977) enforce a model smoothness constraint. Although other constraints are available, we use this constraint because it is easy to implement and yields stable solutions that can map spatially varying geological media reasonably well. In equation (1), the regularization parameters are given by the matrix **W**, which consists of a finite-difference approximation to the Laplacian (∇^2) operator and the trade-off parameter λ. This latter parameter is used to control the amount of smoothness to be incorporated into the model. In its selection, we note that a large parameter produces a highly smooth model, but the model shows poor dependence on the data. A small parameter, on the other hand, gives a superior data fit, but the resulting model may be too rough and nonphysical. Following Newman and Alumbaugh (2000), equation (1) is minimized multiple times with different trade-off parameters that are fixed, and the smoothest model that provides an acceptable match to the data within observational errors is selected as the optimal result.

To ensure that the inverted conductivity is positive, a lower bounding constraint is implemented in the minimization of equation (1). This constraint lets the user designate the lowest conductivity value that the model can attain on a cell-by-cell basis. This constraint is actually implemented by inverting for the logarithm of the parameters (see Newman and Alumbaugh, 2000; Newman et al., 2002).

Because of the size of the 3D inverse problem, gradient methods are the only practical methods for minimizing equation (1). The method of steepest descent is the easiest and simplest gradient method to implement. Unfortunately, it usually converges very slowly in practice. A better approach is the method of nonlinear conjugate gradients (NLCG), first proposed by Fletcher and Reeves (1964) for nonlinear optimization, later improved by Polyak and Ribière (1969), and recently implemented in 2D and 3D MT inversion algorithms (see Newman and Alumbaugh, 2000; Rodi and Mackie, 2001). The method is closely related to the linear CG method of Hestenes and Stiefel (1952) and is in fact identical if the cost functional is quadratic. We refer interested readers to the above references, where more information on the NLCG method can be found with specific details required for the MT data inversion, including efficient evaluation of the cost functional, its gradient, and practical line-search procedures required by this minimization method.

WASTE-SITE MODEL STUDY

To demonstrate the accuracy of the 3D MT inversion algorithm, as well as gain insight into what aspects of the pit and underlying geology that can be resolved in the inversion of the field data, a model of the waste site was constructed (Figure 5). Synthetic data for the model were computed on multiple data profiles at the earth's surface ($\{-100 \text{ m} < x < 100 \text{ m}\}$; $\{-100 \text{ m} < y < 100 \text{ m}\}$) at 5-m intervals in x and y coordinate directions over four frequencies that span 230 to 20 kHz; these frequencies are similar to those used in the actual field survey. The total number of data points inverted was 25 600,

which were generated from the 3D MT finite-difference modeling code of Mackie et al. (1994). Five percent Gaussian noise, based on the impedance of a 200-ohm-m half-space, was then added to the data. Additional details of the model include a 2-m-thick, 50-ohm-m overburden that covers the waste; a 500-ohm-m gravel and coarse sand layer of 19 m depth extent; and a lower 25-ohm-m half-space, representing the conductive tertiary sand, clay, and coal units known to lie beneath the actual waste site. Two pits with resistivities of 20 and 50 ohm-m are included in the model.

xy-section, z=2.5m
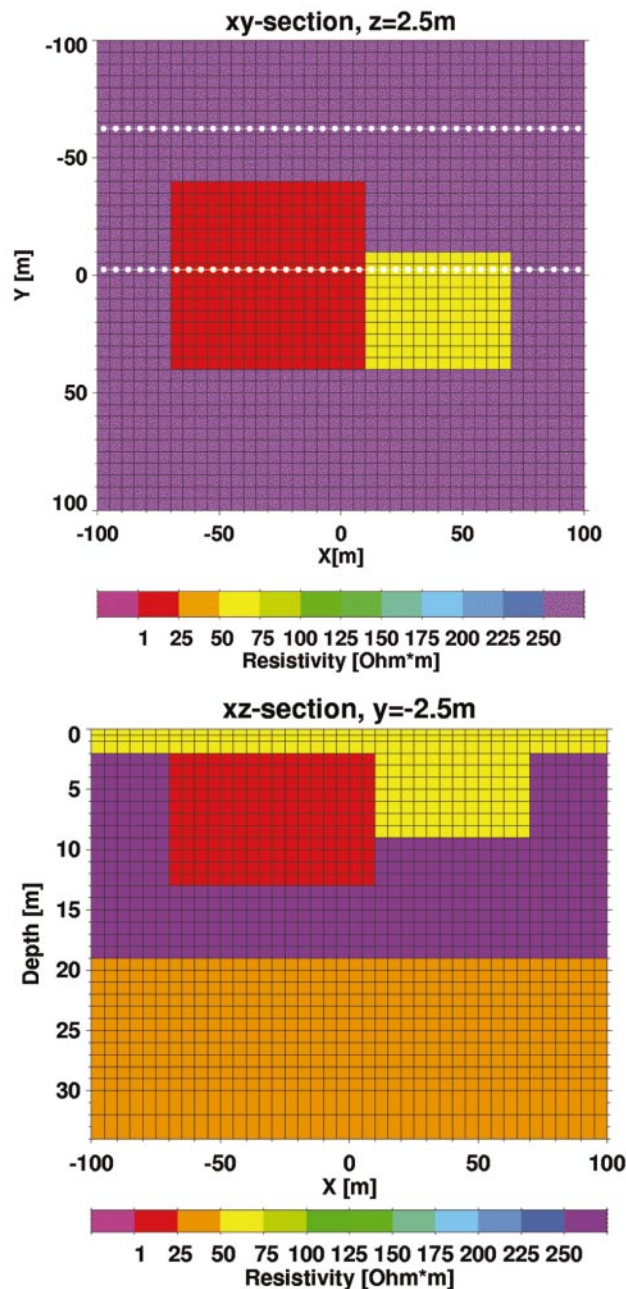
xz-section, y=-2.5m

FIG. 5. Two views of a 3D waste site model. The lateral and depth extent of the waste pits is shown at the top and bottom of the figures, respectively. Additional details of this model are described in the text. Profiles $y = -62.5$ m and $y = -2.5$ m are marked (see Figure 7).

To invert the data using the 3D scheme (Newman and Alumbaugh, 2000), we imposed a model parameterization of 132 553 conductivity unknowns on the inversion domain. For the forward modeling problem, a mesh of 277 875 cells was used for computing predicted data and cost functional gradients. Because of the mesh size, the inverse modeling domain is a subset of the forward modeling problem. This should not cause problems in the inversion process, provided the imaging volume is of sufficient size, where the background model is fixed outside of the imaging volume. This background model, also used to launch the inversion, consists of a 200-ohm-m half-space. Approximately five days of processing time were required to invert the data at a fixed regularization parameter using 252 processors on the Sandia National Laboratories Ascii Red machine.

Figures 6 and 7 show images of the waste site at different depths and cross-sections, where only the off-diagonal components of the impedance tensor were inverted. An examination of the synthetic data arising from the waste model (Figure 5) demonstrated that the Z_{xx} and Z_{yy} elements are a fraction of the size of Z_{xy} and Z_{yx} elements. Only over the corners of the waste pits do the ratios between $|Z_{xx}|/|Z_{xy}|$ and $|Z_{yy}|/|Z_{yx}|$ approach 0.3. Away from the corners, these ratios range from 0.1 to 0.01. For this reason we ignore the diagonal elements of the impedance tensor in the inversion. Note also that the diagonal elements are not available in the field data, discussed below. Sixty-eight inversion iterations were required, reducing the weighted square error (WSE), the first term in equation (1) normalized by the number of data values, from 24 to a final value of 1.2, slightly above the target value of one. When this target value is achieved, the data have been fit statistically to within the estimated noise. The regularization parameter λ used in the inversion was set to a value of one. To achieve the target WSE of one in equation (1) requires running the inversion using a smaller regularization parameter. We did not pursue this because the benefit in improving the reconstruction quality was judged to be minimal compared to the computational costs involved. Data fits along the profile $y = -2.5$ m are shown in Figure 8 for the Z_{xy} and Z_{yx} impedance values, demonstrating the inversion algorithm is nicely fitting the observations in the presence of significant noise.

Features of the model that are recovered include the lateral extent of the pits, the overburden, and the basal conductor outside the pits. The fact that we cannot recover the basal conductor over the pits is not surprising because of conductive screening from the pits. Therefore, in the field data we can expect problems in recovering the basal conductor beneath the waste site. Finally, it appears we have imaged the base of the more conductive pit better than its less conductive and shallower neighbor.

The waste-site model study offers the opportunity to study the bias of 2D data interpretation over the 3D waste site. The 2D inversion scheme (Rodi and Mackie, 2001) used in this analysis, which is also applied to the field data, is similar to the 3D scheme. Both schemes use a nonlinear conjugate gradient technique in the inversion process, with stabilization achieved through regularization based upon a smooth model constraint. Like the 3D scheme, the 2D scheme is executed using several different trade-off parameters to find the optimal data misfit, but it uses apparent resistivity and phase as data

input. Naturally, the 2D scheme is much faster than the 3D version, which requires parallel computing resources for reasonable execution times with extremely large models, hence its appeal. However, the 2D scheme requires two important assumptions. The first is that geological strike is meaningful and the 2D model assumption is valid. The second is that any near-surface statics are confined to the transverse magnetic source polarization. This is a key advantage of a 3D scheme since statics in both source polarizations can be accommodated in the 3D model.

Figure 9 shows a 2D reconstruction along the profile $y = -2.5$ m using the same grid. This profile was selected because it traverses the edge of the shallower pit, and the data will clearly exhibit 3D effects. The 2D reconstruction shows that the base of the more conductive pit has been estimated to extend below 20 m depth, which is significantly deeper than the 13 m shown in Figure 5. This finding persists for different regularization parameters used in the 2D inversions; all models show the same extension of the good conducting structure below the base of the pit. This result could be construed as contamination leaking from the pit into the deeper geological bedding. It could be a cause of significant concern to environmental regulators.

FIELD DATA ANALYSIS

The field data set described above was inverted using 3D and 2D MT inversion imaging schemes to further identify and quantify any advantages 3D data analysis offers over 2D analysis.

As mentioned, the data acquisition in the field survey was made in scalar mode because of the limitation of the RMT
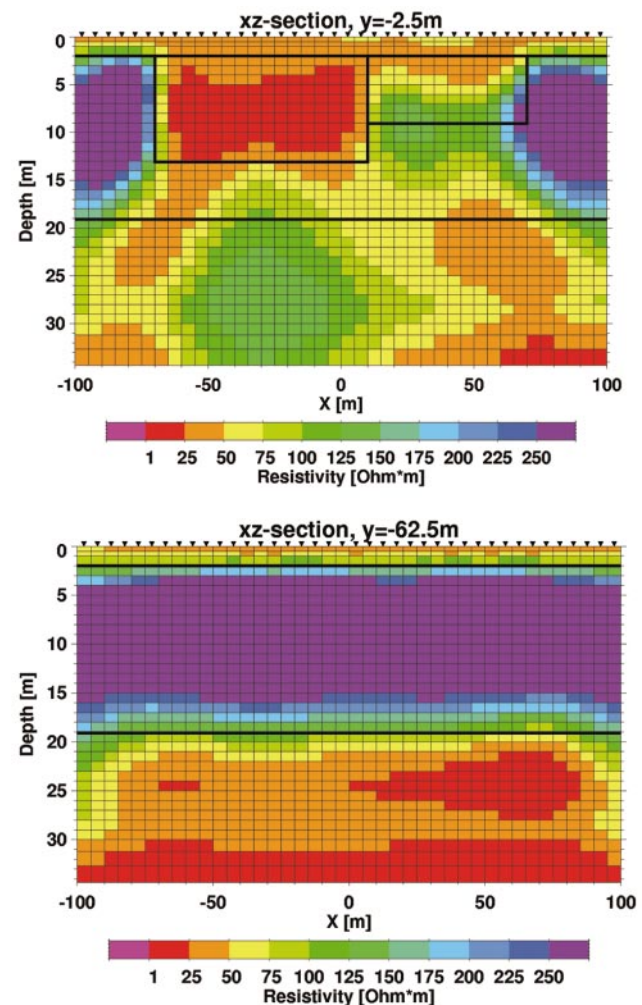

FIG. 6. The 3D reconstructions of the waste-site test model shown at two depths, 2.5 and 12.5 m, below the earth's surface.

FIG. 7. The 3D reconstructions of the waste-site test model, shown at two different cross-sections: $y = -2.5$ and -62.5 m (see Figure 5). Heavy black lines indicate the actual model boundaries.
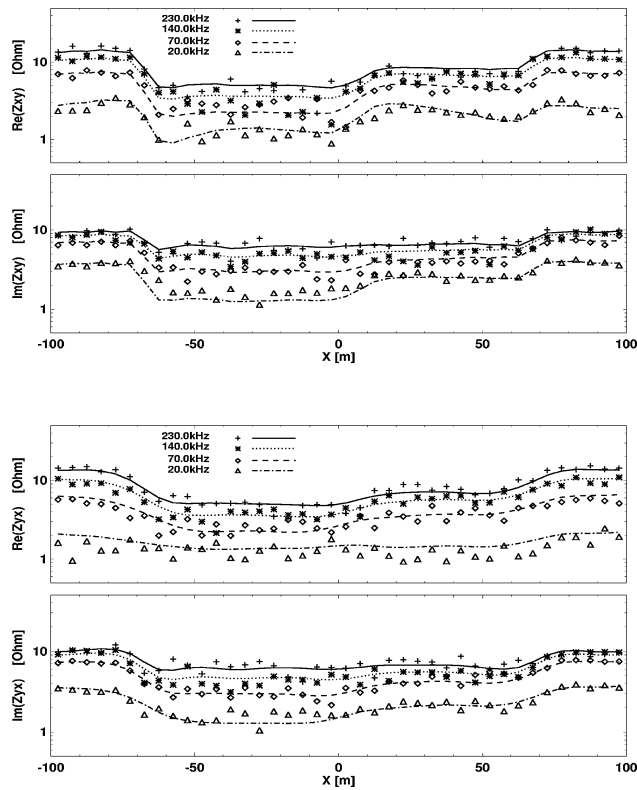
FIG. 8. Data fits of Z_{xy} and Z_{yx} impedance values (real and imaginary) along the profile $y = -2.5$ m. The observations are given by the symbols and the predicted data by the curves at four different frequencies. Because of the log scale and because both the real and imaginary components of the Z_{xy} impedance are negative, we have plotted the absolute value these components in the figure.
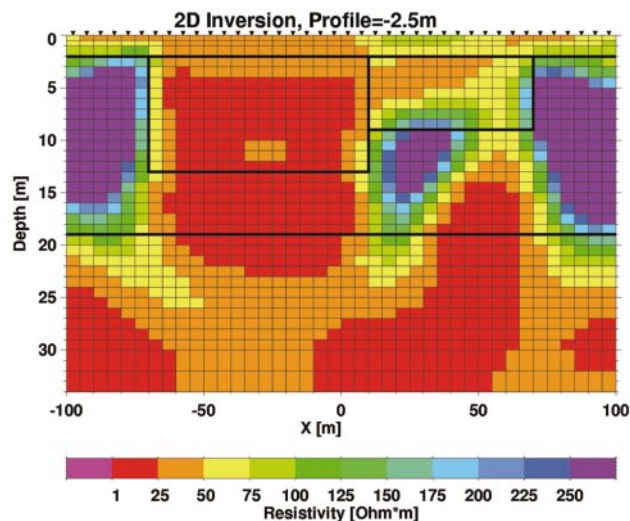

FIG. 9. The 2D reconstruction of the waste-site test model at $y = -2.5$ m. The reconstruction is based on a 500-ohm-m half-space starting model, and achieved a target misfit of 1. It is clear from the reconstruction, that the base of the more conductive pit is too deep, extending below 20 m depth.

measurement device. Here, two separate but independent source polarizations were used. One polarization was assumed to produce the Z_{xy} impedance data values, and the other the Z_{yx} values. Now, if 3D variations in the conductivity beneath the survey area are not too large, we show in the appendix that acquisition of data in scalar mode can be inverted using the 3D MT inversion code described earlier with minimal bias. Recall that this code assumes tensor data. We also justify in the appendix that the scalar field data can be analyzed accurately with a tensor code. This is accomplished by taking the 3D reconstructed model of the field site derived by inverting the field data and demonstrating that the predicted data arising from that model satisfy the necessary conditions given in the appendix. Finally, for 2D data interpretation, acquisition of data in scalar mode presents no problems. In this situation, we assume the impedance data for the two polarizations are decoupled and can be treated separately.

Similar to the inversion of the waste-site test model data, an initial background half-space model of 200 ohm-m was used to launch the inversion using identical meshing. Once again, 252 processors were used to invert the data, requiring several days of processing time for an inversion assuming a fixed regularization parameter. Data errors were assumed to be 5% amplitude of the impedance measurement at each site and frequency. The inversion code was then exercised for three different regularization parameters: 10, 1, and 0.1. All three parameters produced normalized WSE above the target misfit of one. This is not surprising because the data errors used in the inversion are approximate estimates and are clearly non-Gaussian. The smallest regularization parameter produced a 3D model that was judged to be too spatially rough with the smallest data misfit, while the largest parameter yielded a model too smooth with the largest misfit. Hence, our model is based on a regularization parameter of one.

After 42 inversion iterations, the WSE for the 3D data ($\lambda = 1$) drops from an initial value of 433 to less than 3.17. This WSE, normalized by the number of data points, corresponds to the inversion of 4800 data points, or 300 RMT measurement locations over the pit, taken at eight frequencies where the impedance measurement is complex and consisting of real and imaginary parts. Figure 10, compares observed and predicted impedance data along the profile $y = -50$ m in Figure 2. As can be seen, the data fits are good.

Selected cross-sections through the 3D model at $y = -50$ m, $x = 220$ m, and $y = 0$ m are presented in Figure 11. The waste pit is clearly indicated in the 3D image sections, where the resistivity of the pit is less than 50 ohm-m. However, there is no indication of any deeper conductive geological horizons or beds beneath the pit. This does not come as a surprise because of the pit's conductive screening; conductive screening was also demonstrated in the waste-site model study.

Corresponding 2D images for identical profiles are shown in Figure 12. The 2D results were based upon the same starting model used in the 3D inversion, a 200-ohm-m half-space. Normalized WSE error levels for the 2D inversions are around 4.62 for the selected profiles. However, it is difficult to make a direct comparison to the 3D WSE error, which is smaller. The 3D results are based on a data misfit for all measurement points acquired over the pit, while the 2D misfits are based on selected data profiles. Moreover, the 3D and 2D error measures are based on different data types and data weights. We

recall that the impedance is inverted directly upon in the 3D case; in the 2D case, the data are apparent resistivity and phase.

A possible source of error in the 2D imaging results may arise from the geological strike direction assumed for the waste pit. The strike direction can be inconsistent with the polarization directions of the radio transmitters used in the survey, along the different data profiles. This certainly appears to be the situation near some of the lateral pit boundaries in Figure 2. Note also the strike direction is assumed to rotate 90° for the image taken at $x = 220$ m, in comparison to the top and bottom images shown in Figure 12. As already mentioned, this is not an issue for analyzing the data in three dimensions, but it is in two dimensions. Nevertheless, the waste pit is also indicated in all of the 2D images, which agrees quite well with the corresponding 3D images in the near surface where good data coverage exists. Both 3D and 2D imaging results also confirm a lateral pit boundary in the southeastern region of the survey area ($x < 35$ m). However, there is an important difference between the 3D and 2D images. Lateral regions within the 3D image, with no data coverage, show little or no change from the starting model. In contrast, the 2D scheme shows changes. Apparently, these changes are required to reduce the misfit between the observed and the predicted data. They may also be related to the 2D scheme compensating for the 3D nature of the data set and the improper assumptions regarding geological strike. To clarify this situation, however, more analysis of 2D inversion applied to different 3D data sets is necessary. Such analysis is outside the scope of this paper.
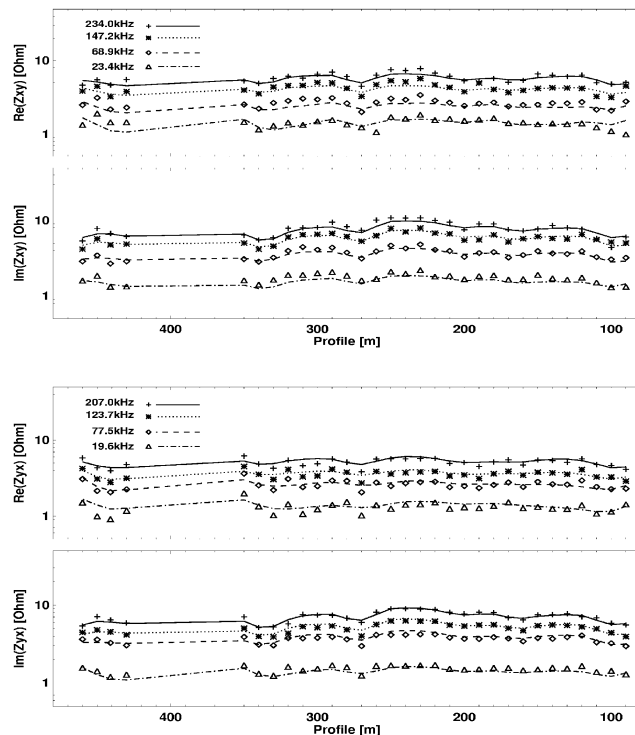
In all of these images over the pit, the 3D results have apparently imaged its base at approximately 16 m depth ($\rho < 50$ ohm-m), which is about 3 to 4 m more than indicated with borehole sampling. In contrast, the 2D results show the base to extend beyond 20 m depth, and this depth appears to be a far greater overestimate, and concurring with our findings from the waste-site model study. Like the 3D results, the 2D results do not indicate any conductive horizons related to the deeper background geology. Because of the pit's conductive screening, the lowest frequency (VLF: 19.6 kHz) used in this study has limited penetration depth. Unfortunately, there exist no civil or military transmitters at frequencies below 19.6 kHz that could have been used to achieve the required penetration depths.

Measurements taken outside the pit along a reference profile can be used to produce a better starting model of the geological media hosting waste site. Our goal is to produce a 3D image of the waste site that is consistent with the background

FIG. 10. Comparison between observed and predicted impedance data (real and imaginary components of Z_{xy} and Z_{yx}) after 42 3D inversion iterations. Symbols mark the observed data; lines mark the calculated 3D data at $y = -50$ m in Figure 2.
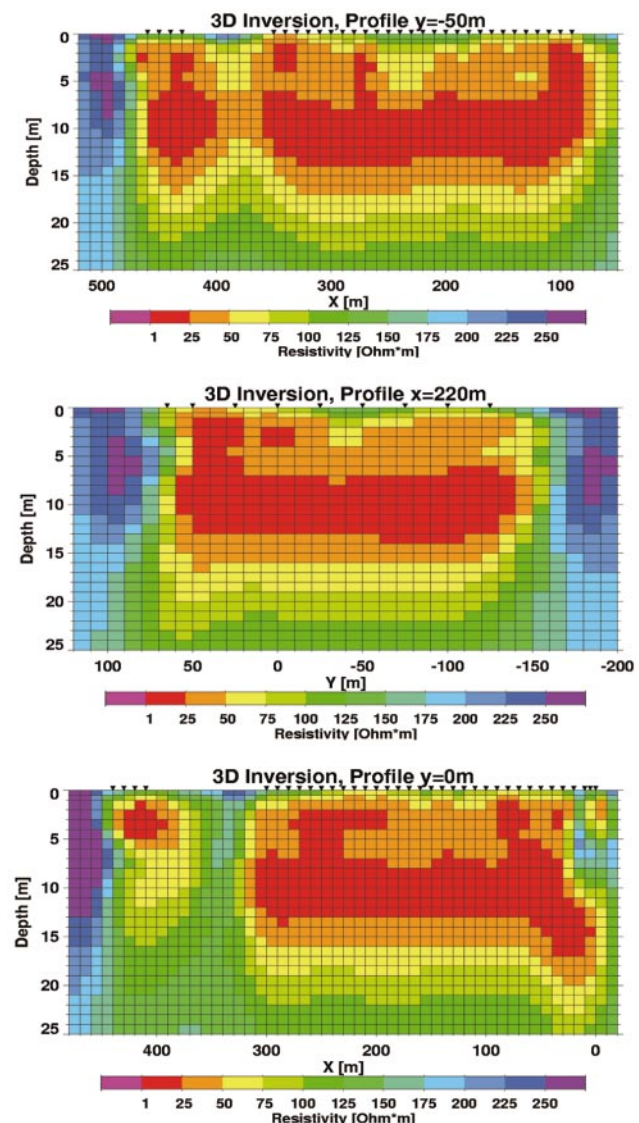

FIG. 11. Three-dimensional inversion results based on a 200-ohm-m half-space starting model for selected profiles.

geology. Figure 13 shows a 2D inversion of data collected along the reference profile in Figure 2. In this case the penetration depth is large enough since there is no screening effect from the conductive waste. The inversion clearly maps the overburden and resistive gravels hosting the pit. More importantly, a deeper geological horizon near 20 m depth is indicated, corresponding to the conductive brown coal, clays, and tertiary sands, shown in the geological cross-sections in Figure 3. This deeper horizon is also indicated at 20 m depth from an electrical dc sounding taken outside the pit along the reference profile.

We now can construct a background geological model of the site that will serve as a starting model for the 3D inversion of the field data set. This two-layered model consists of a 200-ohm-m gravel layer, 20 m thick, and a 25-ohm-m basal conductor, representing brown coal, clay, sand. The 3D image produced from this starting model is shown in Figure 14.
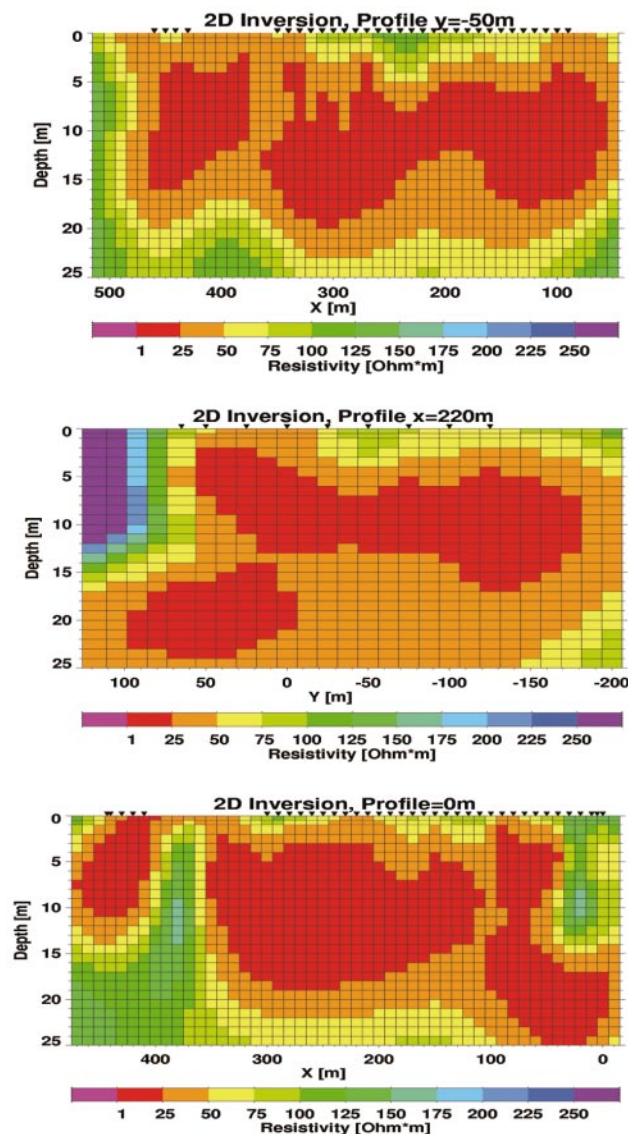
With this background model we produce a sharper image of the pit and estimate the base of the pit to be near 13 m depth, which agrees much better with borehole data. In the shallow parts of the section less than 10 m depth, however, there is good agreement with the 3D image based on the 200-ohm-m half-space starting model in Figure 11. These findings can also be visualized in three spatial dimensions in Figure 15, which shows the estimated pit volume for the two different starting models. With the layered half-space starting model, the pit volume is estimated to be 603 600 m³; for the half-space it is 936 400 m³, assuming $\rho < 50$ ohm-m. Given the layered background model is more appropriate for the site, the 3D image that incorporates it constitutes our final 3D model of the waste site.

CONCLUSIONS

Even with the recent advancements in 3D MT inversion, nonuniqueness and solution uncertainty issues remain a problem. Our 3D results clearly show the benefit of incorporating as much a priori information on the geological background within the inversion process. As an example, by extending the measurements into the surrounding undisturbed region outside the waste pit, we can construct a background geological starting model that addresses the inadequacy of the field data and significantly improves the quality of the image at and below the base of the pit.

The results of our analysis demonstrate some of the possibilities of 3D MT inversion. Since 3D inversion is now an area of active research by others in the MT community (see Mackie et al., 2001), we can expect its application to become more frequent. Hence, one can expect the full benefits of 3D inversion to become even more obvious as it is applied to wider and different types of MT data sets.

FIG. 12. Two-dimensional inversion results based on a 200-ohm-m half-space starting model for selected profiles.
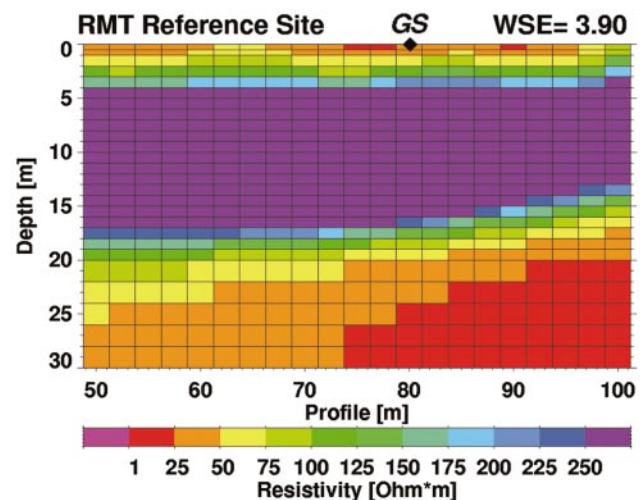

FIG. 13. The 2D resistivity image of the background electrical resistivity outside the pit, obtained from a data profile taken outside and south of the pit (see Figure 2). The data are fit to within WSE of 3.90. Because of noise associated with this profile, transverse magnetic mode data were not used in the inversion. A geoelectric sounding (GS) at $x = 80$ m confirms the presence of the basal conductor near 20 m depth.
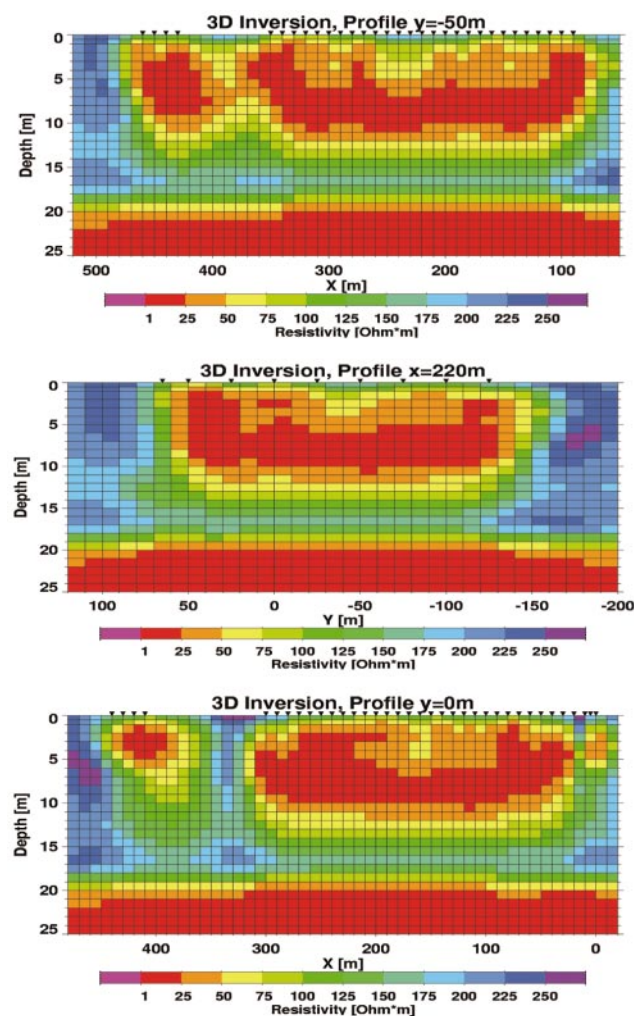
3D Inversion, Profile y=−50m

3D Inversion, Profile x=220m
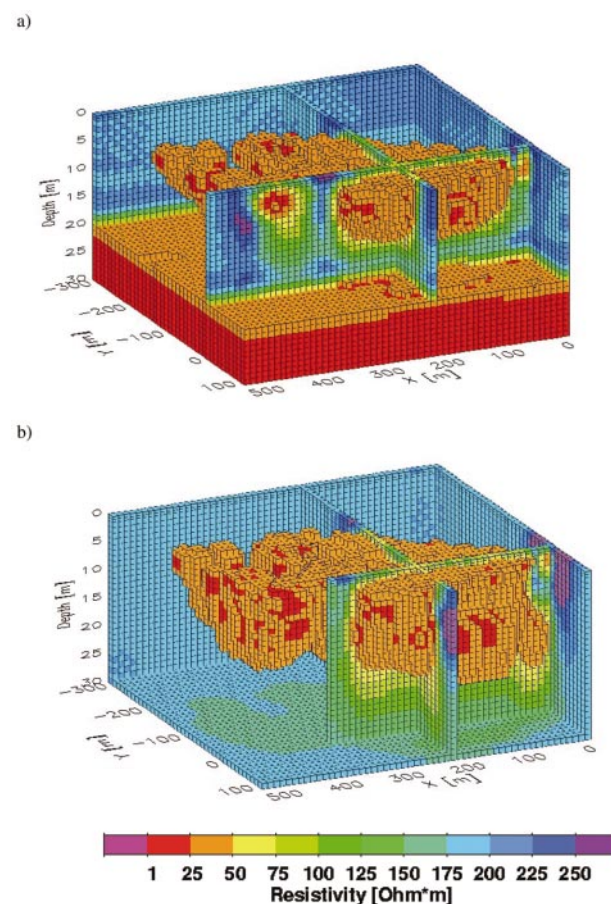
3D Inversion, Profile y=0m

a)

b)

FIG. 15. Three-dimensional renderings of the waste pit for two different starting models: (a) two layers and (b) homogeneous half-space. Resistivities greater than 50 ohm-m have been rendered invisible, except along selected cross-sections.

FIG. 14. Three-dimensional inversion results using a two-layered starting model based on the background geology. The base of the pit is clearly seen in the images in the three selected profiles. Thirty-eight inversion iterations were required to produce these 3D images, where the final weighted square error was 3.53.

REFERENCES

Cagniard, L., 1953, Basic theory of the magneto-telluric method of geophysical exploration: Geophysics, **18**, 605–635.
de Iaco, R., Green, A., and Horstmeyer, H., 2000, An integral geophysical study of a landfill and its host sediments: Eurp. J. Environ. Eng. Geophys., **4**, 223–263.

Fletcher, R., and Reeves, C. M., 1964, Function minimization by conjugate gradients: Computer J., **7**, 149–154.
Geologisches Landesamt Nordrhein-Westfalen, Krefeld, 1986, Ingenieurgeologische karte 1:25 000, Blatt 5007 Köln.
Green, A., Lanz, E., Maurer, H., and Boerner, D., 1999, A template for geophysical investigations of small landfills: The Leading Edge, **18**, No. 2, 248–254.
Greenhouse, J., and Slaine, D., 1983, The use of reconnaissance electromagnetic methods to map contaminant migration: Ground Water Monit. Rev., **3**, 47–59.
Hestenes, M. R., and Stiefel, E., 1952, Methods of conjugate gradients for solving linear systems: J. Res. Nat. Bur., **49**, 409–436.
Mackie, R., Rodi, W., and Watts, M., 2001, 3-D magnetotelluric inversion for resource exploration: 71st Ann. Internat. Mtg., Soc. Expl. Geophys., Expanded Abstracts, 1501–1504.
Mackie, R. L., Smith, T. J., and Madden, T. R., 1994, Three dimensional electromagnetic modeling using finite difference equations: The magnetotelluric example: Radio Science, **29**, 923–936.
McNeill, J. D., and Labson, V., 1991, Geological mapping using VLF radio fields, *in* Nabighian, M. N., Ed., Electromagnetic methods in applied geophysics: Soc. Expl. Geophys., 521–640.
Mueller, I., 1983, Anisotropic properties of rocks detected with electromagnetic VLF: Internat Symp., Field Measurements in Geomechanics, Special Publ., 273–282.
Newman, G. A., and Alumbaugh, D. L., 2000, Three-dimensional magnetotelluric inversion using nonlinear conjugate gradients: Geophys. J. Internat., **140**, 410–424.
Newman, G. A., Hoversten, G. M., and Alumbaugh, D. L., 2002, 3D magnetotelluric modeling and inversion: Applications to sub-salt imaging, *in* Zhdanov, M. S., and Wannamaker, P. E., Eds., Three-dimensional electromagnetics: Elsevier Science Publ. Co., Inc., 127–152.
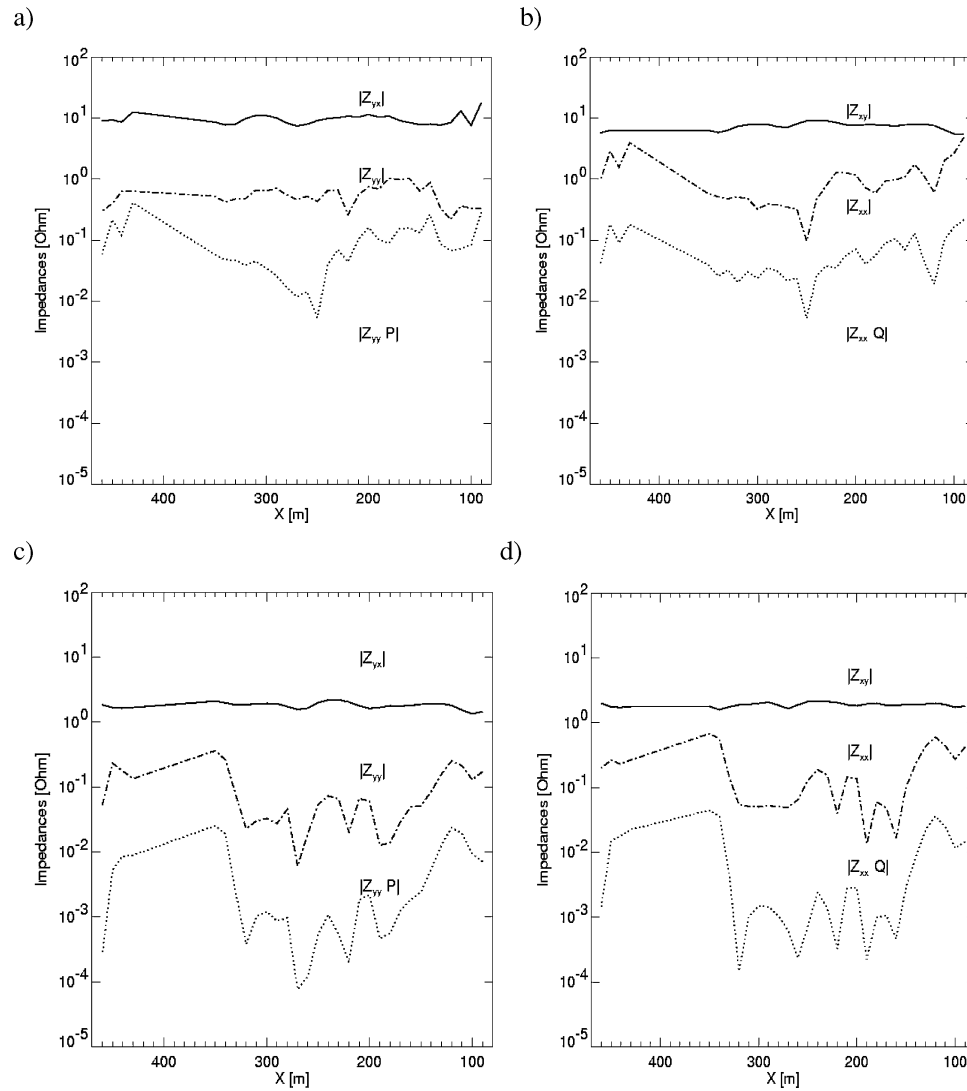
FIG. 16. (a, b) Comparisons between the sizes of the various impedance components $|Z_{yx}|$, $|Z_{yy}|$, $|Z_{yy}P|$ and $|Z_{xy}|$, $|Z_{xx}|$ and $|Z_{xx}Q|$ at 234 kHz for the 3D model illustrated in Figures 14 and 15a. (c, d) The respective comparisons at 16 kHz. The quantities P and Q are ratios of the horizontal magnetic field components H_y/H_x and H_x/H_y, where the profiles correspond to the location $y = -50$ m in Figure 2.

Pellerin, L., and Alumbaugh, D. L., 1997, Tools for electromagnetic investigation of the shallow subsurface: The Leading Edge, **16**, No. 11, 1631–1638.

Polyak, E., and Ribière, G., 1969, Note sur la convergence des méthods conjugées: Rev. Fr. Inr. Rech. Oper., **16**, 35–43.

Rodi, W., and Mackie, R. L., 2001, Nonlinear conjugate gradients algorithm for 2D magnetotelluric inversion: Geophysics, **66**, 174–187.

Smith, J. T., and Booker, J. R., 1991, Rapid inversion of two and three dimensional magnetotelluric data: J. Geophys. Res., **96**, 3905–3922.

Tezkan, B., 1999, A review of environmental application of quasi-stationary electromagnetic techniques: Surv. in Geophys., **20**, 279–308.

Tezkan, B., Goldman, M., Greinwald, S., Hoerdt, A., Mueller, I., Neubauer, F. M., and Zacher, G., 1996, A joint application of radio magnetotellurics and transient electromagnetics to the investigation of a waste deposit in Cologne, Germany: J. Appl. Geophys.,

34, 199–212.

Tezkan, B., Hoerdt, A., and Gobashy, M., 2000, Two dimensional radio magnetotelluric investigation of industrial and domestic waste sites in Germany: J. Appl. Geophys., **44**, 237–256.

Tikhonov, A. N., and Arsenin, V. Y., 1977, Solutions to ill-posed problems: John Wiley & Sons, Inc.

Turberg, P., Mueller, I., and Flury, F., 1994, Hydrological investigation of porous environments by radio magnetotelluric-resistivity (RMT-R 12–240 kHz): J. Appl. Geophys., **31**, 133–143.

Vozoff, K., 1972, The magnetotelluric method in the exploration of sedimentary basins: Geophysics, **37**, 98–141.

——— 1991, Magnetotelluric method, *in* Nabighian, M. N., Ed., Electromagnetic methods in applied geophysics: Soc. Expl. Geophys., 641–712.

Zacher, G., Tezkan, B., Neubauer, F. M., Hoerdt, A., and Mueller, I., 1996, Radio magnetotellurics: A powerful tool for waste-site exploration: Euro. J. Environ. Eng. Geophys., **1**, 135–159.

APPENDIX
TENSOR ANALYSIS OF SCALAR DATA

In magnetotellurics, the horizontal components of the electric and magnetic fields (**E**, **H**) arising from a 3D earth are related to each other through a relationship involving the impedance tensor **Z**, which is a function of position (x, y) and frequency at the earth's surface:

$$\begin{pmatrix} E_x \\ E_y \end{pmatrix} = \begin{pmatrix} Z_{xx} & Z_{xy} \\ Z_{yx} & Z_{yy} \end{pmatrix} \begin{pmatrix} H_x \\ H_y \end{pmatrix}. \qquad \text{(A-1)}$$

The tensor is described by four elements. To recover these elements in an inversion process generally requires that all horizontal components of the electric and magnetic field be measured.

Consider the situation where only the y-component of an electric field is measured along with the x-component of a magnetic field. We define the ratio of these field quantities by the impedance

$$\frac{E_y}{H_x} = Z_{yx}^* = Z_{yx} + \frac{Z_{yy} H_y}{H_x}. \qquad \text{(A-2)}$$

Here, H_y corresponds to the unknown y-component of the magnetic field, unknown because it was not measured. We now define a variable P, which corresponds to the ratio of the horizontal magnetic field components. Specifically, we have

$$P = \frac{H_y}{H_x}. \qquad \text{(A-3)}$$

In general P depends upon the source polarization of the field and 3D earth structure. When the earth is two dimensional and the electric field is polarized along the y-direction, then $P = 0$. However, when the earth is 3D, P is no longer identically zero. From equation (A-2), the condition that must be satisfied to interpret scalar data using an inversion code based on a full tensor formulation is

$$|Z_{yx}| \gg |Z_{yy} P|. \qquad \text{(A-4)}$$

Fortunately, this is a weaker condition than

$$|Z_{yx}| \gg |Z_{yy}| \qquad \text{(A-5)}$$

because, in general,

$$|P| < 1. \qquad \text{(A-6)}$$

Thus, if equation (A-4) is satisfied, we can assume that

$$Z_{yx}^* \approx Z_{yx}. \qquad \text{(A-7)}$$

If we consider E_x and H_y measurement pairs, the analogous condition to equation (A-4) is

$$|Z_{xy}| \gg |Z_{xx} Q|, \qquad \text{(A-8)}$$

where

$$Q = H_x / H_y. \qquad \text{(A-9)}$$

Hence, if equation (A-8) holds, then

$$Z_{xy}^* \approx Z_{xy}. \qquad \text{(A-10)}$$

To test the validity of equations (A-7) and (A-10), we consider the 3D reconstructed model of the waste site shown in Figure 14, which is our favored model of the waste site. We computed the predicted impedance tensor as well as the quantities P and Q at each measurement point. In the computation of P and Q, we assumed knowledge of the field polarization, which is consistent with the RMT data acquisition strategy. For example, when evaluating equation (A-4), we computed P using the predicted magnetic field arising from a y-directed source polarization. For all frequencies and measurement points, computations indicated equations (A-7) and (A-10) are excellent approximations to within 5% error; these conclusions hold as well for other models of the waste site presented in this paper and determined through 3D data inversion. In Figure 16 we show plots of $|Z_{yx}|$, $|Z_{yy}|$, $|Z_{yy} P|$ and $|Z_{xy}|$, $|Z_{xx}|$ and $|Z_{xx} Q|$ for two frequencies (234 and 16 kHz) along the profile $y = -50$ m. Clearly, equations (A-4) and (A-8) are easily satisfied.

If the scalar data are treated exactly, this would involve modification to our 3D inversion scheme. Specifically, we would attempt to minimize the following squared error:

$$\Phi = \left\| Z_{yx}^* - (Z_{yx} + Z_{yy} P) \right\|^2 + \left\| Z_{xy}^* - (Z_{xy} + Z_{xx} Q) \right\|^2. \qquad \text{(A-11)}$$

For the data analysis we present, minimization based on equation (A-11) was determined not to be necessary.